

---

# **MATLAB/Simulink-Based Grid Power Inverter for Renewable Energy Sources Integration**

---

Marian Gaiceanu

Additional information is available at the end of the chapter

<http://dx.doi.org/10.5772/48489>

---

## **1. Introduction**

The main objective of the chapter is the development of technological knowledge, based on Matlab/Simulink programming language, related to grid connected power systems for energy production by using Renewable Energy Sources (RES), as clean and efficient sources for meeting both the environment requirements and the technical necessities of the grid connected power inverters. Another objective is to promote the knowledge regarding RES; consequently, it is necessary to bring contribution to the development of some technologies that allow the integration of RES in a power inverter with high energy quality and security. By using these energetic systems, the user is not only a consumer, but also a producer of energy. This fact will have a direct impact from technical, economic and social point of view, and it will contribute to the increasing of life quality.

The chapter intends to integrate itself into the general frame of the EU energy policies by imposing the global objectives of reducing the impact upon the environment, and promoting the RES for the energy production. At the same time, the chapter is strategically oriented towards the compatibility with the priority requirements from some European programmes: the wide-spread implementation of the distributed energy sources, of the energy storage technologies and of the grid connected systems.

The chapter strategy follows two directions: the first, is the development of knowledge (a study and implementation of a high performance grid-power inverter; the fuel cells technology as RES; the control methods; specific modelling and simulation methods); the second focuses upon the applicative research (a real time implementation with dSPACE platform is provided).

The interdisciplinarity of the chapter consists of using specific knowledge from the fields of: energy conversion, power converters, Matlab/Simulink simulation software, real time

---

implementation based on dSPACE platform, electrotechnics, and advanced control techniques.

## 2. The grid power converter

The increased power demand, the depletion of the fossil fuel resources and the growth of the environmental pollution have led the world to think seriously of other alternative sources of energy: solar, wind, biogas/biomass, tidal, geothermal, fuel cell, hydrogen energy, gas micro turbines and small hydropower farms.

The number of distributed generation (DG) units, including both renewable and nonrenewable sources, for small rural communities not connected to the grid and for small power resources (up to 1000 kW) connected to the utility network has grown in the last years. There has been an increase in the number of sources that are natural DC sources, for instance fuel cells and photovoltaic arrays, or whose AC frequency is either not constant or is much higher than the grid frequency, for instance micro gas-turbines. These generators necessarily require a DC/AC converter to be connected to the grid. Although some generators can be connected directly to the electric power grid, such as wind power driven asynchronous induction generators, there is a trend to adopt power electronics based interfaces which convert the power firstly to DC and then use an inverter to deliver the power to the 50Hz AC grid.

At the international level, SMA Technologies AG ([www.sma.de](http://www.sma.de)) promotes the innovative technology based on the renewable sources. The following results can be mentioned: the stand-alone or grid connected systems by using either a single type of source (Sunny Boy 5000 Multi-String inverter based on the modular concept, Hydro-Boy and Windy Boy) or combined (Sunny Island) including the interconnection of wind turbines, photovoltaics, micro-hydro and diesel generators. It is well-known that for systems efficiency increasing, the inverter is the answer of the problem. With this respect, Sunways ([www.sunways.de](http://www.sunways.de)) adopted the HERIC concept (from the Fraunhofer Solar and Energetic Systems Institute), by using a transformerless inverter, obtaining a 97,33% high efficiency of the inverter for low powers ([www.ise.fraunhofer.de](http://www.ise.fraunhofer.de)). The Master-Slave and Team concepts are embedded in SunnyTeam and Fronius inverters in order to increase the efficiency in the partial load conditions. At world level, the implementation of energetic policies (with respect to renewable sources) has been carried out by performing systems based on a single renewable source. There are such examples in countries all over the world: in Europe, Dewind, Vestas, Enercon, Fronius International GmbH, SMA Technologies AG; Renco SpA, Ansaldo Fuel Cells SpA; in North America-Nyserda, Beacon Power, Magnetek Inc., Sustainable Energy Technology, Logan Energy Corp., IdaTech; Australia-Conergy Pty Ltd, Rainbow Power Company Ltd; and Asia-Nitol Solar, Shenzhen Xinhonghua Solar-Energy Co Ltd).

In EU, the implementation of the energetic policies is based upon a legal document, Norm 2001/77/EC regarding the promotion of the electrical energy produced from renewable sources on the Energy Single Market. The objectives of the Norm provide that till 2020, a contribution of 20% of the total energy consumption shall be covered by energy produced

from renewable sources. The monitoring of this Norm implementation is managed by the EU Energy General Directorate which presents periodical reports on the European researching and development stages. Considering these reports, under the conditions of implementing the DER concept (Distributed/Decentralized Energy Resources), it is obvious that the futurer research activities will be based upon the hybrid systems (wind-photovoltaic, wind-biomass, wind-diesel generator) having the target of the energetic security by removing the disadvantages of using a single renewable source.

The consolidation of the objectives proposed by Norm 2001/77/EC and the extension in more geographical areas are possible only by using hybrid systems.

The EU gives a great importance to the improvement of the energy efficiency and to the promotion of the renewable sources. Related to the above mentioned issues, the objectives of the EU are to produce at least 20% of the gross energy consumption from renewable sources until 2020 (COM, 2006) and to increase the energy efficiency by 20% until 2020 (EREC, 2011). As far as the energy efficiency is concerned, an EU norm aims at a reduction of 9% of the energy losses until 2020 (EREC, 2008)

### **2.1. A generic topology of the RES integration**

In the context of the international scientific studies related to the development of new alternative solutions for electrical energy production by using renewable energy sources (RES), the aim of this chapter is to contribute to these studies by evaluating and working out the possible concepts for stand-alone and grid connected operating interface of these hybrid systems and the efficient and ecologic technologies to ensure an optimal use of the sources (solar energy, wind energy, hydrogen energy by using fuel cells, hydro-energy, biomass) in industry and residential buildings. The battery and the fuel cells are also meant to be reserve sources (which ensure the additional energy requirements of the consumers and the supply of both the residential critical loads and the critical loads of the hybrid system-auxiliary circuits for fuel cell start-up and operating), increasing the safety of the system. The fuel cell integration is provided by using a unidirectional DC/DC converter (to obtain regulated high voltage DC), an inverter and a filter in order to accommodate the DC voltage to the required AC voltage (single phase or three phase). The bidirectional DC/DC converter (double arrow, Fig.1) is used in order to charge/discharge the batteries (placed in order to increase the energy supply security and to improve load dynamics). The unidirectional DC-DC converter prevents the negative current going into the fuel cell stack. Due to the negative current, the cell reversal could occur and damage the fuel cell stack. The ripple current seen by the fuel cell stack due to the switching of the boost converter (unidirectional DC/DC converter) has to be low.

### **2.2. Three-phase versus single phase**

Firstly, the problem of choosing the number of phase for the front end converter is a matter of power. In this case, the three-phase line should be used for a 37kVA power converter.

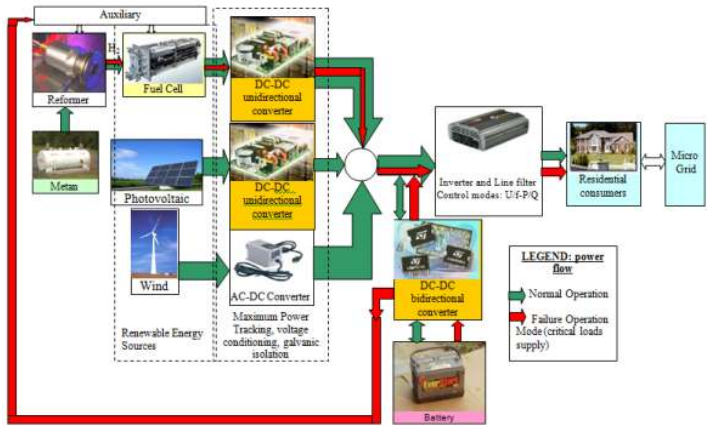


**Figure 1.** A generic topology of the RES integration

Secondly, in case of using balanced three phase AC loads, the possibility that low frequency components to occur in the fuel cell input current is reduced.

### 2.3. System description

The proposed way of the efficient integration of RES is illustrated in Fig.1. With this respect only one inverter is used in DC-AC conversion for interfacing the stand-alone or grid-connected consumer (Gaiceanu, *et al.*, 2007b). By its control, the inverter can ensure the efficient operation and the accomplishment of the energy quality requirements related to the harmonics level. The hybrid system can ensure two operation modes: the normal one, and the emergency one (as backup system).

#### 2.3.1. Operation modes

There are four modes of operation:

- **Direct Supply from Utility:** consists of direct supply of the residential consumers from Utility via the Static Switch;
- **Precharge Operation:** The DC capacitors in the inverter part of the Power Conditioning System (PCS) can be precharged from the AC busutility. After the DC capacitors are charged, the inverter can be switched on. As soon as it is running, the inverter by itself will keep the DC capacitors charged to a DC level higher than the No-Load level of the Solid Oxide Fuel Cell (SOFC). During the precharge operation, the residential consumers will still be supplied from Utility;
- **Normal Operation:** The PCS converts the DC energy from the SOFC into AC and feeds the Utility and the eventual residential consumers.
- **Island Operation(failure operation mode):** If the Utility goes out of tolerance during normal operation, the PCS will change to island operation. The PCS converts the DC from SOFC and battery and supplies the critical loads.



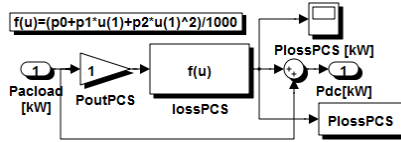


**Figure 3.** The energetic model of the PCS

In the Fig.3. the energetic component of the PCS block is presented. By knowing the total inverter losses at critical power,  $P_{loss,inv}^{tot}$ , the corresponding DC power can be obtained:

$$P_{DC} = P_{out,inv} + P_{loss,inv}^{tot} \tag{3}$$

The input and the output inverter powers are related to the inverter efficiency:

$$\eta_{inv} = \frac{P_{out,inv}}{P_{DC}} \tag{4}$$

By taking into account the power requirements of the auxiliary circuits, which are supported only by the battery pack in critical load case during the fuel cell start-up, the corresponding DC power is (Fig.4):

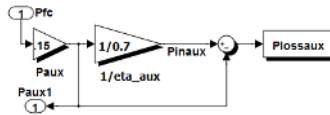


**Figure 4.** The power losses of the auxiliary power circuits

$$P_{DCi} = P_{DC} + P_{aux} \Rightarrow P_{DCi} = P_{DC} + 0.15P_{FC}^{critical} \tag{5}$$

The necessary energy of the battery pack is obtained as:

$$W_{batt} = \int_0^t P_{DCi} d\tau \tag{6}$$

The blowers have been considered as main auxiliary loads; the value of  $\eta_{aux} = 0.7$  for the equivalent efficiency of the auxiliary power circuits has been considered. In the Fig.4c, the power losses of the auxiliary power circuits have been deducted.

$$\Delta P_{loss,aux} = P_{out,aux} \left( \frac{1}{\eta_{aux}} - 1 \right) \tag{7}$$

*PCU Matlab/Simulink simulator results*

Based on the PCUMatlab/Simulink simulator (Fig.2, Fig. 5a), the required capacity and energy of the battery have been obtained (Fig. 5b)

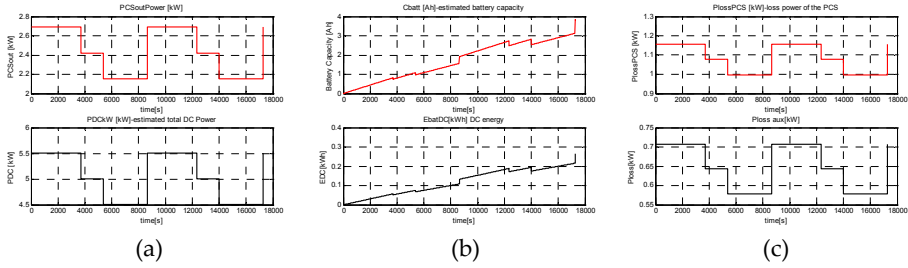


**Figure 5.** (a) The load power PCSoutPower [kW], the estimated total DC power PDC[kW], including the auxiliary power loss; (b) the required capacity and energy of the battery, respectively; (c) the losses of the PCS and the auxiliary power losses.

### 2.3.1.2 The Normal operation mode

#### A. The Fuel Cell Power Conditioning System

The fuel cell power conditioning system consists of fuel cell stack and DC power converter. The fuel cell is an electrochemical device which produces DC power directly, without any intermediate stage. It has high power density and zero emission of green house gases. Fuel cell stacks were connected in series/parallel combination to achieve the desired rating. The main issue for the fuel cell power converter design is the fuel cell current ripple reduction. The secondary issue is to maintain a constant DC bus voltage. The former is solved by introducing an internal current loop in the DC/DC power converter control. The latter design requirement is solved by DC voltage control.

##### A.1 The Fuel cell stack Matlab/Simulink based model

The polarization curve of the SOFC is based on Tafel equation. The output voltage of the SOFC is built taking into account the Nernst instantaneous voltage equation  $E_0 + a \ln(P_{H_2} P_{O_2}^{1/2})$ , the activation overvoltage  $b \ln(i)$ , the voltage variation due to the mass transport losses  $c \ln\left(1 - \frac{i}{i_{lim}}\right)$  and the ohmic voltage drop  $Ri$  (Candusso D., et al. 2002). The first three terms are multiplied by No, number of series cells, in order to obtain the fuel cell stack mathematical model.

The parameters of the Tafel equation are the load current, the temperature and the pressures of the hydrogen and oxygen. The demanded current of the fuel cell system is limited between  $\pm I_{fc}^{limit}$  at a certain hydrogen flow  $q_{H_2}^{in}$  value (Padulles, et al., 2000):

$$\frac{0.8q_{H_2}^{in}}{2K_r} \leq I_{fc}^{in} \leq \frac{0.9q_{H_2}^{in}}{2K_r} \quad (8)$$

The Simulink model of the FC Power System before starting must be initialized (based on *Ifc\_init.m* file, Fig.6) from the Fuel Cell data initialization block (Fig.5). In order to obtain the

demanded current between certain limits, an adequate Matlab function has been created(Fcn).

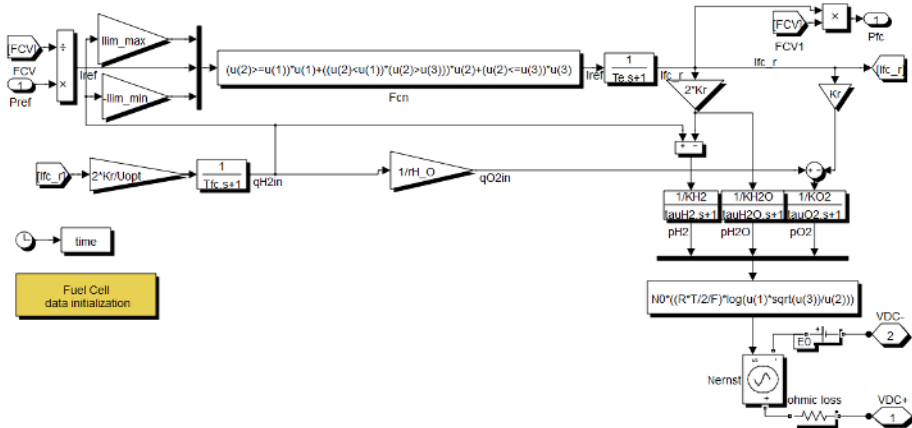


Figure 6. The Simulink model of the solid oxide fuel cell stack

*Ifc\_init.m*

```

prate=80000; % [W]   Rated power, Pref=80000; % [W]   Real power reference

T=1273; % [K]   Absolute temperature, F=96487; % [C/mol]   Faraday's constant

R=8314; % [J/(kmol.K)] Universal gas constant, E0=1.18; % [V]   Ideal stand potential

N0=384; %   Number of cells in series inside the stack, Kr=0.995*10^(-5); % kmol/(s.A), Constant, Kr = N0/4F

Umax=0.9; % Maximum fuel utilization , Umin=0.8; % Minimum fuel utilization Uopt=0.85; % Optimal fuel utilization ,

%Value molar constants:

KH2=8.43*10^(-4); % kmol/(s atm) - for hydrogen

KH2O=2.81*10^(-4); % kmol/(s atm) - for water

KO2=2.52*10^(-3); % kmol/(s atm) - for oxygen

tauH2=26.1; % s - Response time for hydrogen flow

tauH2O=78.3; % s - Response time for water flow

tauO2=2.91; % s - Response time for oxygen flow

r=0.126; % ohm - Ohmic loss

Te=0.8; % s - Electrical response time

Tfc=5; % s - Fuel processor response time

rH_O=1.145; % - Ratio of hydrogen to oxygen

PF=1.0; % - Power factor

% demanded current limits of the fuel cell system, Iref, fuel cell

Ilim_max=Umax/2/Kr;

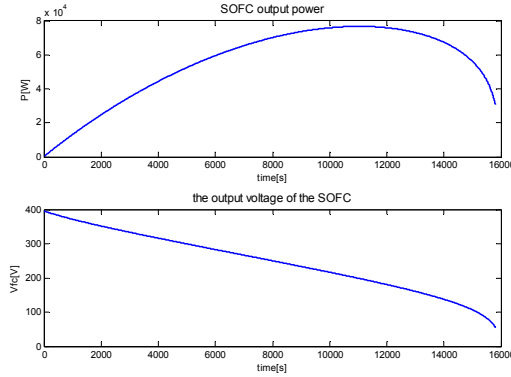
Ilim_min=Umin/2/Kr;
    
```

Figure 7. SOFC Initial data (Padulles; Zhu)



### A.2 Simulation results

By using the implemented Simulink model (Fig.5), the output voltage and the output power have been obtained, as shown in Figure 7.



**Figure 8.** The solid oxide fuel cell characteristics: the power and the output voltage

### A.3 Mathematical modeling of the DC-DC power converters for fuel cells and energy storage elements integration: Boost and Buck-Boost power converters

In order to obtain a constant DC voltage, a boost power converter has been taken into consideration (Figure 9), operating in continuous conduction mode (CCM).

The method of the time averaged commutation device is applied to the unitary modeling of the power converters presented in Fig. 9 (Ionescu, 1997).

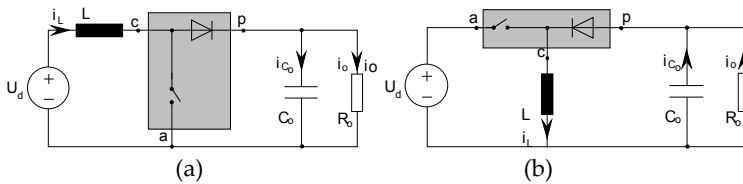


**Figure 9.** DC-DC non-isolated converters: (a)boost; (b) buck-boost

During the  $DT_s$  period, the active device is ON and the passive device is OFF. During the  $(1-D)T_s$  period, the active device is OFF and the passive device is ON, while the passive terminal  $p$  is connected to the common terminal  $c$ . The duty factor is denoted  $D$  and  $T_s$  is the switching period. Taking into consideration the above mentioned hypotheses, the following instantaneous currents can be deduced:

$$i_a(t) = \begin{cases} i_a(t) & \text{during } DT_s \\ 0 & \text{during } (1-D)T_s \end{cases}, i_p(t) = \begin{cases} 0 & \text{during } DT_s \\ i_c(t) & \text{during } (1-D)T_s \end{cases} \quad (9)$$

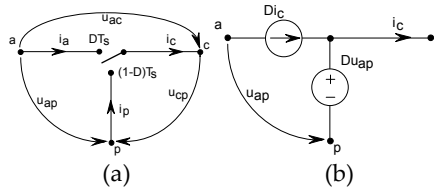


**Figure 10.** (a) The equivalent three-pole for the commutation device; (b) the equivalent diagram of a time averaged model over a switching period (Ionescu, 1997)

In the similar manner, the specific instantaneous voltages are obtained:

$$u_{cp}(t) = \begin{cases} u_{ap}(t) & \text{during } DT_s \\ 0 & \text{during } (1-D)T_s \end{cases}, u_{ac}(t) = \begin{cases} 0 & \text{during } DT_s \\ u_{ap}(t) & \text{during } (1-D)T_s \end{cases} \quad (10)$$

If averaging is carried out over a period of switching time, equations (9) - (10) will assume the equivalent form of the currents

$$\begin{cases} i_a = Di_c \\ i_p = (1-D)i_c \end{cases} \quad (11)$$

and of voltages, respectively:

$$\begin{cases} u_{cp} = Du_{ap} \\ u_{ac} = (1-D)u_{ap} \end{cases} \quad (12)$$

where, for the sake of convenience, values such as  $i_a$  are still considered as time averaged values for a period of switching time.

To demonstrate the validity of the time-averaged commutation device model, the mathematical models for DC –DC converters, boost and boost-buck are considered.

#### A.4 The Boost converter

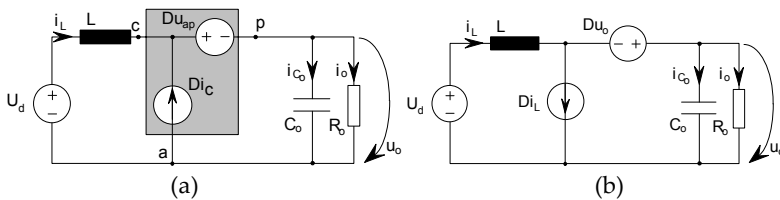


**Figure 11.** The equivalent structure of the boost converter (Ionescu, 1997)

- From the Fig.11a, the following equivalent relations are obtained:

$$\begin{cases} i_c = -i_L \\ u_{ap} = -u_o \end{cases} \quad (13)$$

- By applying the first Kirchhoff's theorem to the Fig.11b, the first differential equation that characterizes the output voltage dynamic state  $\dot{v}_0$  is obtained:

$$(1-D)i_L = C_o \frac{du_o}{dt} + \frac{u_o}{R_o} \text{ or, in the final form } \frac{du_o}{dt} = \frac{1}{C_o} \left[ (1-D)i_L - \frac{u_o}{R_o} \right]$$

- By applying the second Kirchhoff's theorem, the second differential equation that characterizes the inductor current dynamic state,  $\dot{i}_L$ , is obtained:

$$U_d + Du_o = L \frac{di_L}{dt} + u_o \text{ or, in the form } \frac{di_L}{dt} = \frac{1}{L} [U_d - (1-D)u_o]$$

The commutation mathematical model in state space form will be as following:

$$\begin{bmatrix} \dot{i}_L \\ \dot{u}_0 \end{bmatrix} = \begin{bmatrix} 0 & -(1-D)\frac{1}{L} \\ (1-D)\frac{1}{C_o} & -\frac{1}{RC_o} \end{bmatrix} \begin{bmatrix} i_L \\ u_0 \end{bmatrix} + \begin{bmatrix} \frac{1}{L} \\ 0 \end{bmatrix} U_d \tag{14}$$

The voltage  $u_0$  is considered controlled output.

- By vanishing the differential terms, the steady-state regime is obtained from the above deduced dynamic state-vector  $\dot{x} = \begin{bmatrix} \dot{i}_L & \dot{u}_0 \end{bmatrix}^T$ , ∴

$$\begin{cases} U_0 = U_d \frac{1}{1-D} \\ I_o = (1-D)I_L = \frac{U_o}{R_o} \end{cases} \tag{15}$$

### B. Battery Power Conditioning System

The Battery Power Conditioning System consists of a battery pack and a DC-DC power converter. The NiMH battery produces a variable DC power. The battery pack has as main task to deliver the critical load power (Fig.1).

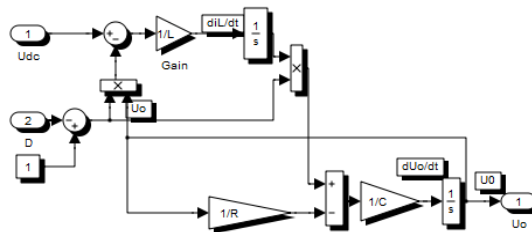
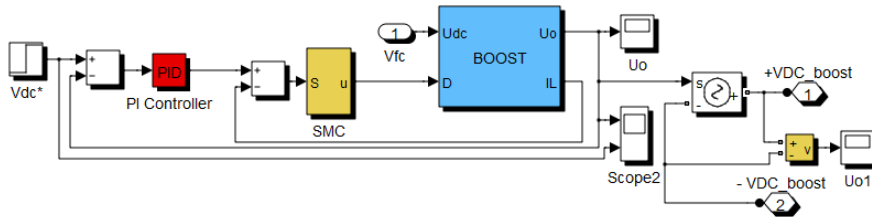


Figure 12. The Simulink diagram of the boost converter

Therefore, individual batteries are connected in series/parallel combination to achieve the desired rating. The Matlab/Simulink battery model from the Mathworks has been used. The main issue for the battery power converter is to charge/discharge battery according to the available flow power. The problem is solved by introducing an internal current loop (Fig.12) in the DC/DC power converter control (Fig.13).

*B1. Simulink implementation of the SMC control diagram for DC-DC Boost Power Converter*

In (Gulderin Hanifi, 2005) it is shown that the existence condition of the SMC is that the output voltage must be greater than the input one.



**Figure 13.** Control of the boost converter: Cascaded DC link voltage loop and current control

The DC-link voltage control is based on the Proportional Integral (PI) controller having  $k_p=0.00001$  and  $k_i=0.01$  as parameters. The circuit parameters of the boost converter are  $L_{boost}=80*1e-6$  [H],  $C_{boost}=3240*1e-6$  [F],  $R_{boost}=20[\Omega]$ .

The current loop is based on the sliding mode control (Fig.14); the Matlab Simulink implementation is shown in Fig.13.

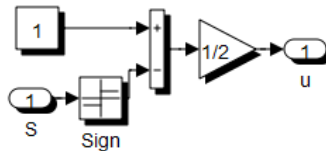


**Figure 14.** Sliding mode current control

The sliding mode surface  $S$  consists of the current error:

$$S = i_L^* - i_L, \tag{16}$$

which vanishes ( $S=0$ ) in order to force the system to enter the sliding surface. The sliding mode controller has two functions: the control function and the modulator one. Therefore, the output control of the SMC is the duty cycle,  $D$ , of the boost power converter.

$$D = \frac{1}{2}(1 - \text{sign}(S)) \tag{17}$$

In order to follow the current reference, the output DC voltage must be greater than the following limit:

$$U_0 \geq \frac{3}{2} \sqrt{(V_{grid}^{max})^2 + (L_{inv} \omega I_{grid}^{max})^2} \tag{18}$$

where the RMS grid voltage is  $V_{grid}^{max}$ , the maximal grid current is  $I_{grid}^{max}$ ,  $\omega$  is the frequency (rad/s), and  $L_{inv}$  is the phase inductance (Candusso D, et al., 2002).

After the simulation, results have confirmed the benefits of SMC control (Fig.15a). The output voltage of the converter reaches and stabilizes at the reference value of 690 V at a time of  $2 \cdot 10^{-2}$  s (Fig.15b), a very short time in comparison with other control methods, while the error voltage is zero (Fig.15c).

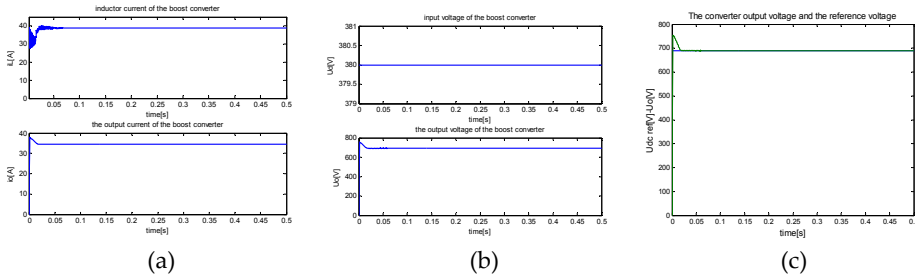


**Figure 15.** a) The converter output voltage and the reference voltage; b) Input voltage variation; c) The current and the voltage at converter output

The fundamental purpose of using this converter is to raise the voltage from the fuel cell generator. Thus, the battery pack delivers 380Vdc, being the input voltage of the boost converter; the output voltage must be compatible with that of the three-phase voltage source inverter input, i.e. 690Vdc.

The advantages of this type of control are: stability, robustness and a good dynamics.

*B1. The mathematical model of the Buck-Boost power converter*

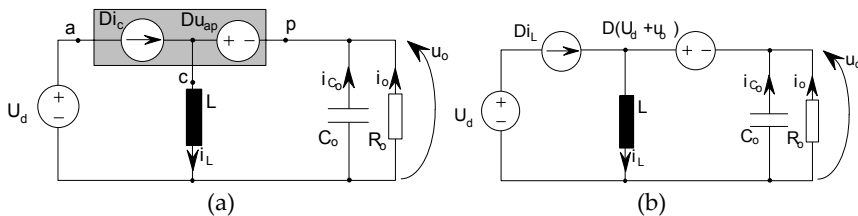


**Figure 16.** Equivalent structure of the boost-boost converter (Ionescu, 1997)

- From the Fig.16a, the following equivalent relations are obtained:

$$\begin{cases} i_c = i_L \\ u_{ap} = U_d + u_o \end{cases} \tag{19}$$

- Following the above procedure applied to the boost power converter, the dynamic model of the buck boost converter is deduced :

$$\begin{cases} \frac{di_L}{dt} = \frac{1}{L} [DU_d - (1-D)u_o] \\ \frac{du_o}{dt} = \frac{1}{C_o} \left[ (1-D)i_L - \frac{u_o}{R_o} \right] \end{cases} \tag{20}$$

and the steady state regime, respectively:

$$\begin{cases} U_o = U_d \frac{D}{1-D} \\ I_o = (1-D)I_L = \frac{U_o}{R_o} \end{cases} \tag{21}$$

*B.2. The Simulink model of the Buck Boost power converter*

Both the buck boost power converter and the current controller have been implemented and simulated in Simulink (Fig.17).

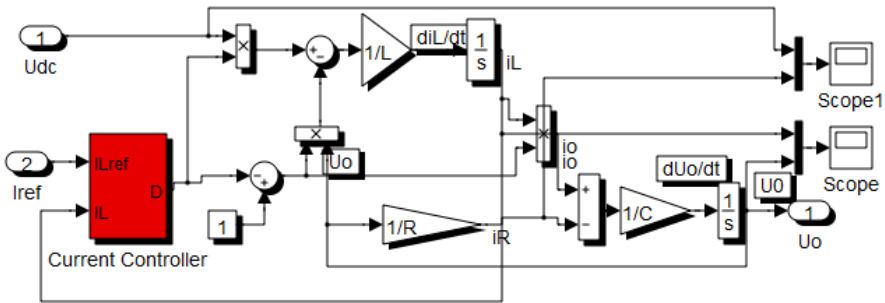


**Figure 17.** Simulink diagram of the buck-boost converter

*B.2.1 The Current Controller*

By imposing the inductor current reference (ILref, Fig.18), the current controller will assure the fast reference tracking at the same time with delivering the appropriate duty cycles (D). By introducing an anti-parallel diode for each active power device, a bidirectional buck-boost converter is obtained.

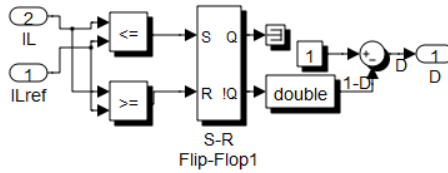


**Figure 18.** Buck-boost current controller

The buck-boost converter is necessary to connect the battery stack ( $U_a=U_{dc}$ ) to the power inverter system and it comes into operation when the electrical power demanded by consumers is higher than the electrical power obtained from the fuel cell generator. Another reason for the use of the buck-boost converter is to recharge the batteries from the other available sources. The circuit parameters of the buck boost power converter are  $L=100 \times 10^{-5}$  [H],  $C=500 \times 10^{-8}$  [F],  $R=50$  [ $\Omega$ ].

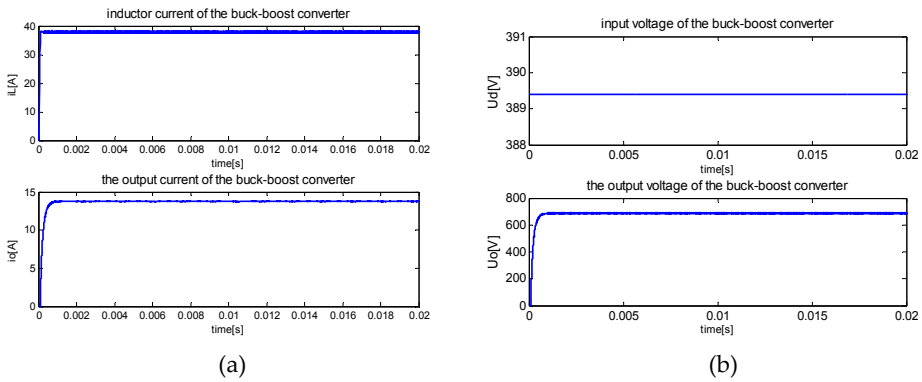


**Figure 19.** The simulation results of the buck-boost power converter

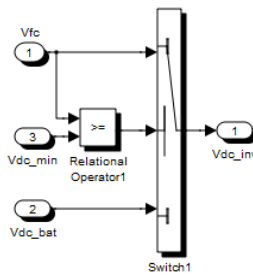


**Figure 20.** The Power Source Selector

Thanks to the buck boost current controller, the actual inductor current follows the reference current. In the output current a delay of 0.001 s could be found (Fig.19a). The input voltage of the buck-boost converter,  $U_a$ , is about 390 Vdc and it is delivered from the battery stack, while the output voltage,  $U_o$ , is boosted at 690 Vdc (Fig.19b).

C. Power Source Management (PSM) (Fig.20)

The purpose of the PSM is to assure an adequate DC-link voltage to the power inverter from both power source generators: the solid oxide fuel cell stack and the battery pack.

The final DC link voltage (VDC\_inverter, Fig.21) is delivered to the Voltage Source Inverter (VSI) by the Power Source Management block (Fig.20).

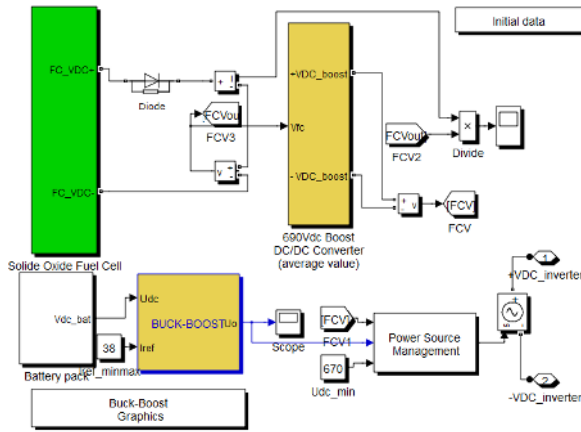


Figure 21. The power sources interconnection

3. Inverter modelling and control

The fundamental types of control can be classified into two categories: current control and voltage control. When the inverter is connected to the network, the network controls the amplitude and frequency of the inverter output and the inverter operates in current control mode. The classical current control can lead to other control methods can be obtained such as active and reactive power control/voltage control. If the network being power injected is not available due to improper network parameters, the inverter will autonomously supply the load; consequently it adequately supplies the alternative voltage in amplitude and frequency and it is not affected by network black outs. In this case, the inverter will control the voltage. The 50 Hz frequency is assured by a phase-locked loop (PLL) control. The grid converter is a full-bridge IGBT transistor-based converter and it normally operates in inverter mode such that the energy is transferred from the hybrid source to the utility grid and/or to the load. When the system is operating in **grid-connected mode**, the PLL tracks the grid voltage to ensure synchronization; but when the system enters in **islanding mode of operation**, the VSI can no longer track the grid characteristics. As seen in Fig. 22, the PLL for the VSI changes the frequency which is sent to the pure integrator for angle calculation by switching between the frequency from the filter and that from another fixed reference. In the islanding mode of operation the VSI needs to have an external frequency reference provided,  $\omega_{fixed}$  (Fig.22). The PLL for the VSI is the main catalyst for the re-synchronization and re-closure of the system to the Utility once disturbances have passed. The frequency from the filter is used during the grid-connected mode.



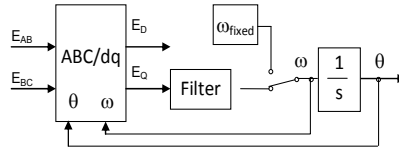


Figure 22. VSI PLL showing switched reference frequency

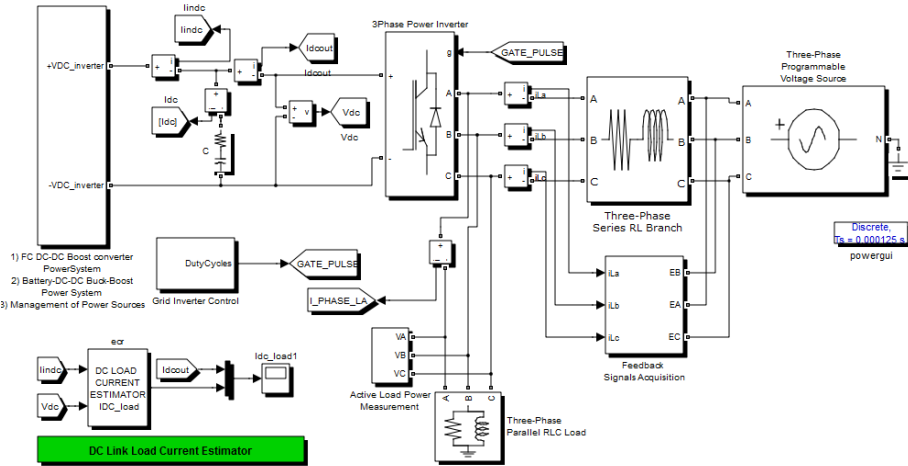


Figure 23. The Simulink model of the Grid Power Inverter for Renewable Energy Sources Integration with DC link Load Current Estimator

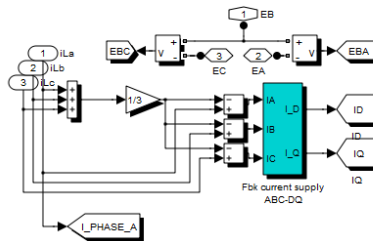


Figure 24. Feedback Signals Acquisition measurement block

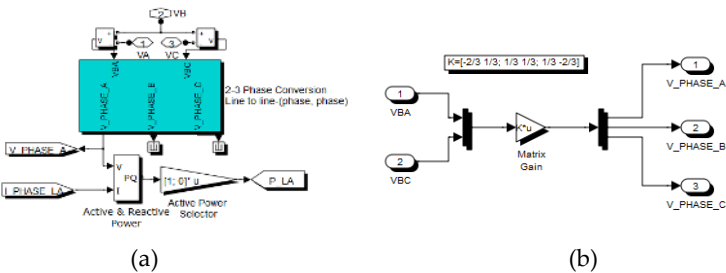
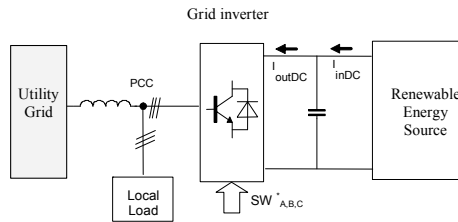
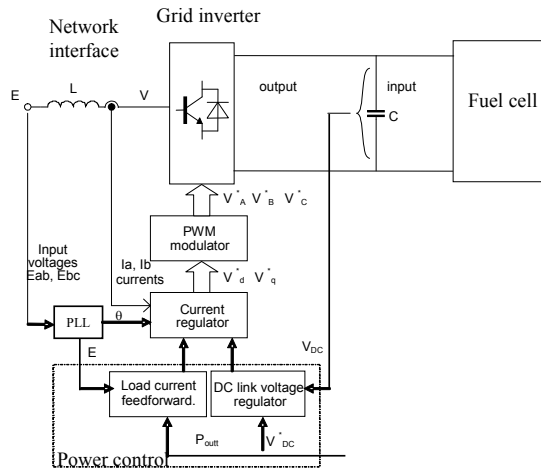


Figure 25. (a)Active Load Power Calculation block; (b) 2/3 phase transformation block



**Figure 26.** Block diagram of RES, Grid inverter, Local Load and grid interconnection

The Grid Power Inverter for Renewable Energy Sources Integration is of 37kVA and delivers the power to the grid (simulated as three-phase programmable voltage source in Fig. 23) and the necessary power to the consumers (simulated as three-phase parallel RLC load in Fig. 23). There is an adequate boost inductor (three-phase series RL branch, Fig. 23) between the grid and the inverter. In order to calculate the  $dq$  components of the grid current, ( $I_D$ ,  $I_Q$ ), the Feedback Signals Acquisition block is used (Fig. 24). Through the implemented Simulink blocks (Figs.25a, 25b), the active power of the load is known.



**Figure 27.** Proposed control system for grid inverter

### 3.1. The grid inverter control

The grid inverter control block delivers the corresponding duty-cycles to the Power Inverter (Gate\_Pulses in Fig.23 or  $SW_{ABC}$  in Fig. 26). To achieve full control of the utility-grid current, the DC-link voltage must be boosted to a level higher than the amplitude of the grid line-line voltage. The power flow of the grid side inverter is controlled in order to keep the DC-link voltage constant. The structure of the DC/AC converter control system is shown in Fig. 27. The control structure of the power inverter is of vector control type and it uses the power balance concept (Sul and Lipo, 1990). Therefore, the load current feedforward component

was introduced in order to increase the dynamic response of the bus voltage to load changes.

On the basis of the DC voltage reference  $V_{DC}^*$ , DC voltage feedback signal ( $V_{DC}$ ), AC input voltages ( $E_{ab}$  and  $E_{bc}$ ), current feedback signals ( $I_a$ ,  $I_b$ ), and the load power signal (got through a load power estimator) (Gaiceanu, 2004a), the Digital Signal Processor-based software operates the control of the power inverter (DC link voltage and current loops) system and generates the firing gate signals to the PWM modulator (Fig.27). The grid connected PWM inverter supplies currents into the utility line by maintaining the system power balance. By controlling the power flow in power conditioning system, the unidirectional DC-link voltage can be kept at a constant value. Using the synchronous rotating frame the active power is controlled independently by the  $q$ -axis current whereas the reactive power can be controlled by the  $d$ -axis current.

The control of the grid inverter is based on the minor current loop in a synchronous rotating-frame with a feedforward load current component added in the reference, completed with the DC voltage control loop in a cascaded manner. The outer loop controller consists of two parts: the phase-locked loop (PLL) and the DC link voltage controller. The former, the PLL, is used to extract the fundamental frequency component of the grid voltages and it also generates the corresponding quadrature signals in  $d$ - $q$  synchronous reference frame,  $E_d$ - $E_q$ , which are necessary to calculate the active and reactive power of the grid. The latter monitors the power control loop. The power control of the PWM inverter, is based on the power detection feedforward control loop and the DC-voltage feedback control loop (Fig.27). The main task of the voltage controller is to maintain the DC link voltage to a certain value. Another task is to control the grid converter power flow. The task of the DC link voltage and of the current regulation has been accomplished by means of the Proportional-Integral (PI) controller type, because of its good steady-state and dynamic behavior with the power inverter. It is important to underline that the PI controller performances are parameters sensitive, because of its design procedure, based on the DC bus capacitor and inductor values. However, in these specific applications, the system parameters values are known with reasonable accuracy. The design of the linear control systems can be carried out in either the time or the frequency domain. The relative stability is measured in terms of **gain margin**, and **phase margin**. These are typical frequency-domain specifications and should be used in conjunction with such tools as Bode plot.

The transfer function of the PI controller (Gaiceanu, 2007b) has the form:

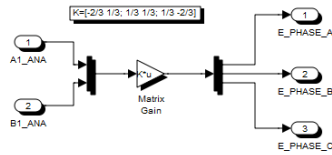
$$C_{PIc}(s) = K_{pc} \left( 1 + \frac{1}{T_{ic}s} \right) \quad (22)$$

The calculation of the PI controller coefficients,  $K_{pc}$  (proportional gain) and  $T_{ic}$  (integral time), is done imposing the phase margin  $\phi_{mc}$  (in radian) and the bandwidth,  $\omega_c$ , (in radian per second). Imposing these two conditions, the following relations for  $K_{pc}$  and  $T_{ic}$  are obtained (Gaiceanu, 2007b):

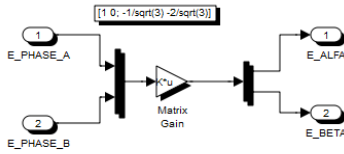
$$\begin{cases} T_{ic} = \frac{1}{\omega_c \cdot \tan\left(-\frac{\pi}{2} - \phi_{mc}\right)} \\ K_{pc} = \frac{-T_{ic} \cdot \omega_c^2 \cdot L}{\sqrt{1 + (T_{ic} \cdot \omega_c)^2}} \end{cases} \quad (23)$$

### 3.2. The Phase Locked Loop (PLL)

A phase locked loop (PLL) ensures the synchronization of the reference frame with the source phase voltages by maintaining their *d* component at zero ( $E_d=0$ ) through a PI controller; the grid frequency is delivered by knowing the line-line grid voltages (EBA, EBC), as in Figs.28, 29.



(a) line-line to three phase



(b) (A,B,C)-(alfa, beta)

**Figure 28.** The transformation of the coordinates

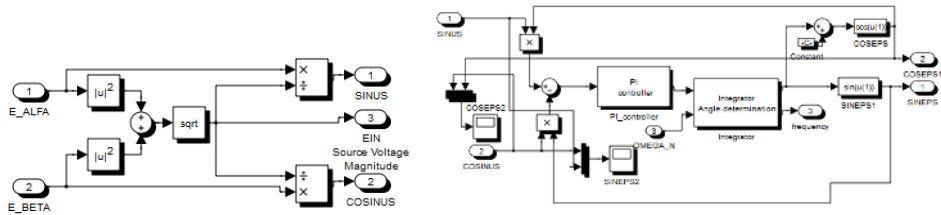


**Figure 29.** (a) Calculus of the required PLL's input trigonometric functions (b) PLL

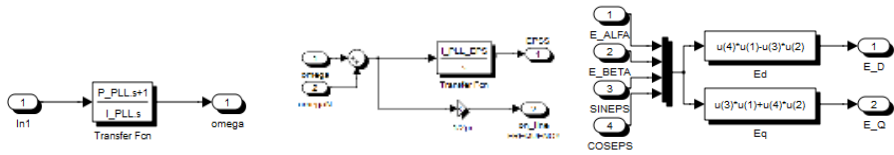


**Figure 30.** (a) The PI regulator of the PLL (b) The integrator for angle calculation (c)  $dq$  grid voltage components: ED, EQ

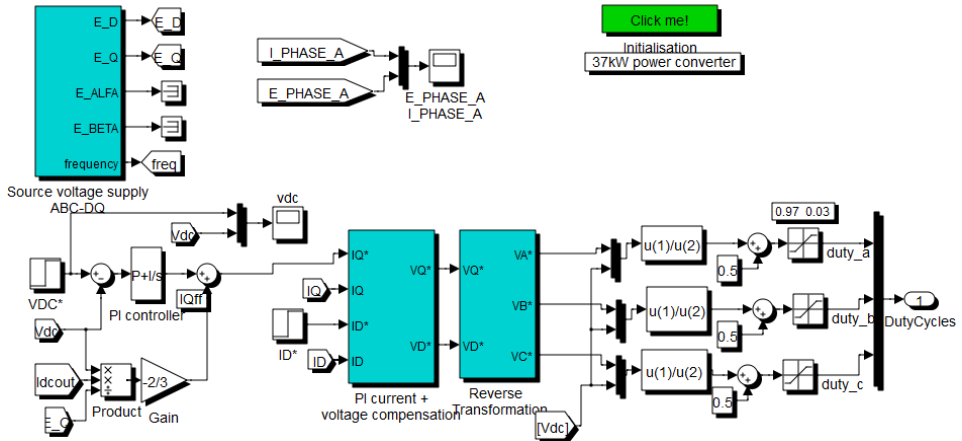


**Figure 31.** The Simulink structure of the DC/AC converter control system

### 3.3. The current controllers

By using a decoupling of the nonlinear terms, the cross coupling (due to boost input inductance) between the  $d$  and  $q$  axes was compensated. To decouple current loops, the proper utility voltage components have been added (Gaiceanu, 2004b) (Fig 32).

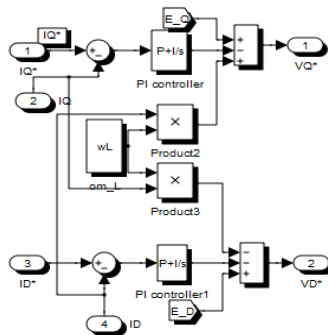


**Figure 32.** Voltage decoupling control

Fig.33 shows the Simulink implementation of the reverse transformation from synchronous reference frame (d,q) to fixed reference frame (A,B,C) through the (alpha,beta) transformations.

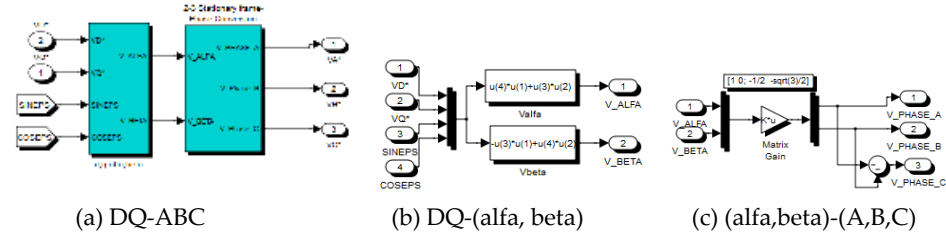


Figure 33. Reverse voltage transformation

### 4. The DClink current estimator

The load power ( $P_{load}=P_{out}$ ) is calculated from the load inverter terminals. Another method is to estimate the load power from the DC link, indirectly, through a first or second order DC load current estimator (Gaiceanu, 2004a). The power feedforward control (Uhrin, 1994) allows the calculus of the input current reference based on the generated power, and it satisfies the power balance in a feedforward manner. By using the load feedforward control, the input reference of the current is changed with load, thus it is obtained a better transient response. The increase in the power response of the DC-AC inverter leads to the possibility of reduction the size of the DC link capacitor by maintaining the stability of the system.

The block diagram of the second degree estimator is presented in the Fig. 34, where the input needs the measure of the DC link voltage  $V_{dc}(p)$  and the calculus of the input ac load current component  $I_q$ . The output of the estimator is the estimated DC link load power  $\hat{P}^{dcout}(p)$ .

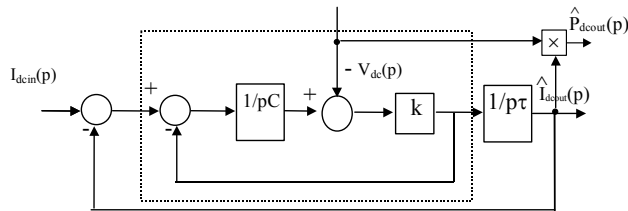


Figure 34. The second order dc link load power estimator

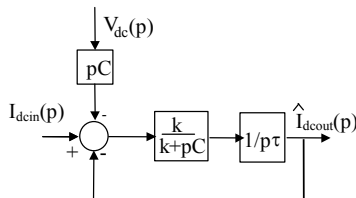
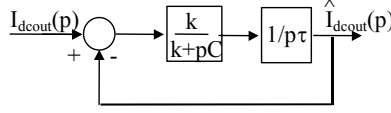
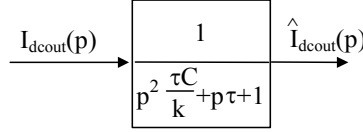


Figure 35. The redrawing estimator

The estimator (Fig. 34), after some manipulations (Fig.35), gets the form presented in the Fig. 36.



**Figure 36.** The simplified diagram of the DC load



**Figure 37.** The final second order estimator

Using Laplace transform the DC link voltage equation gets the form

$$pCV_{dc}(p) = I_{dcin}(p) - I_{dcout}(p) \quad (24)$$

or:

$$I_{dcin}(p) - pCV_{dc}(p) = I_{dcout}(p) \quad (25)$$

This means that the block diagram from Fig.35 can be redrawing as in Fig. 36.

#### 4.1. Calculus of the estimator parameters

The problem consists of the calculation of the parameters  $k$  and  $\tau$  such that the error between the estimated DC load current  $\hat{I}_{dcout}(p)$  and the actual DC load current  $I_{dcout}(p)$  to be insignificant. The closed loop transfer function of the estimator, (Fig.37), derived from Fig.36, is given by:

$$G(p) = \frac{\hat{I}_{dcout}(p)}{I_{dcout}(p)} = \frac{1}{p^2 \frac{\tau C}{k} + p\tau + 1} \quad (26)$$

Considering a step variation for the  $I_{dcout}(p)$ , by setting:

$$I_{dcout}(p) = \frac{I_{dcout}}{p} \quad (27)$$

the estimated DC load current gets the form

$$\hat{I}_{dcout}(p) = I_{dcout} \frac{1}{p(p^2 \frac{\tau C}{k} + p\tau + 1)} \quad (28)$$

The usual form of the equation (28) is given by

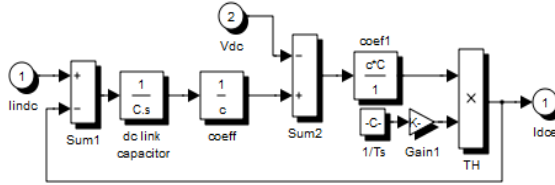


**Figure 38.** Simulink implementation of the DC link load current estimator

$$\hat{I}_{dcout}(p) = I_{dcout} \frac{1}{p(T_0^2 p^2 + 2\xi T_0 p + 1)} \tag{29}$$

where the damping factor is

$$\xi = \frac{\tau \cdot \omega_0}{2} \tag{30}$$

and the pulsation factor

$$\omega_0^2 = \frac{1}{T_0^2} = \frac{\tau}{k \cdot C} \tag{31}$$

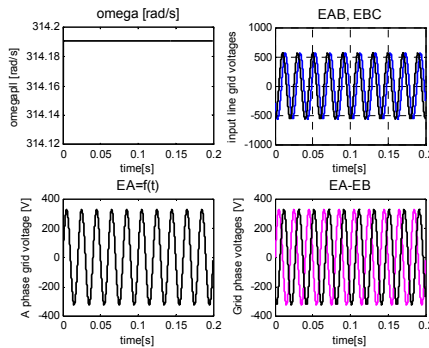


**Figure 39.** The frequency of the line voltage. The acquisition of the grid line voltages (EAB,EBC) and the phase transformation (EA, EB).

The parameters  $k$  and  $\tau$  are chosen such that the response  $\hat{I}_{dcout}(p)$  to have an acceptable overshoot

$$\sigma = e^{-\frac{\pi\xi}{\sqrt{1-\xi^2}}}, \tag{32}$$

a small step time response



$$t_a = \frac{\ln(0.05\sqrt{1-\xi^2})}{-\xi \cdot \omega_0}, \tag{33}$$

and a minimum output noise.

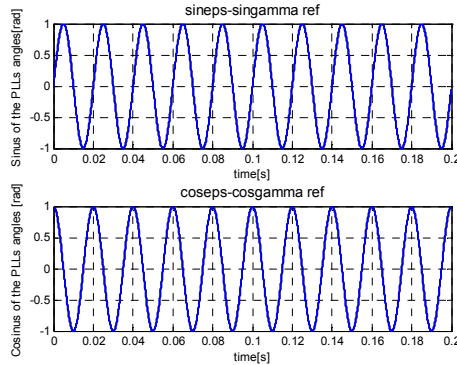


**Figure 40.** The input and the output signals of the PLL circuit

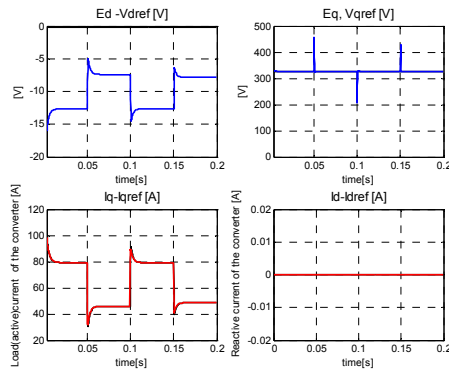


**Figure 41.** The comparison of the grid voltage and the converter voltage ( $E_d, V_{dref}$ ), ( $E_q, V_{qref}$ ) and the performances of the current controllers

An advantage of the estimated method is that there is no ripple presence in the feed-forward reference current of the source side. The small reference current ripple is delivered from the output of the DC link voltage controller.

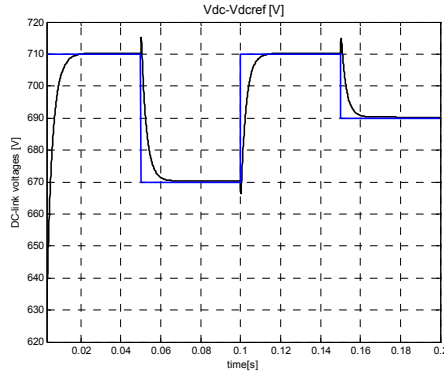


Figure 42. DC link voltage reference, Actual DC link voltage.

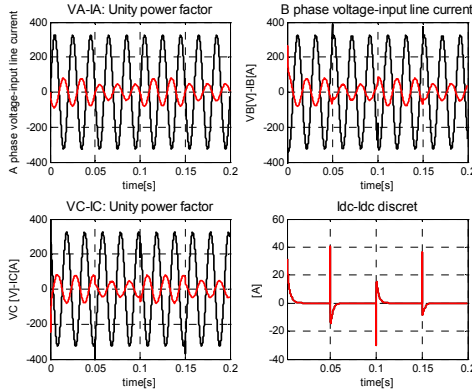
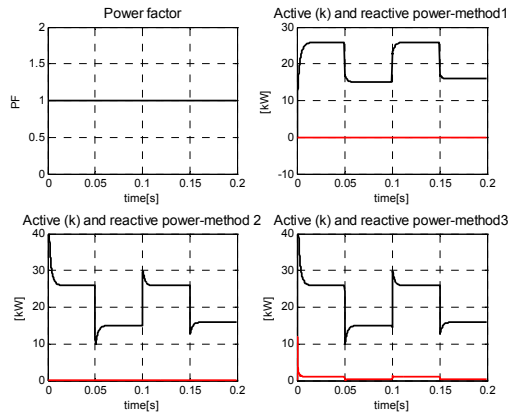


Figure 43. Waveforms showing the unity power factor operation: A, B, C phase grid voltages and the corresponding IA, IB, IC line currents. Simulation results. Idc- the current through the DC link capacitor

### 4.2. Simulation results

Fig. 41 shows the comparison of the grid voltage and the converter voltage ( $E_d, V_{dref}$ ): the  $E_d$  component is 0 and the voltage  $V_{dref}$  is calculated as  $V_{dref} = \omega_m * L_{in} * I_{qN} + E_d$  in steady state regime (Gaiceanu, 2007a). The voltages  $E_{qref}$  and  $V_{qref}$  have the same value of 326.55[V].



**Figure 44.** The unitary power factor operation and comparison results of the three methods of active and reactive power deduction

The reference and actual  $d$  axis current waveforms ( $I_d$ - $I_{dref}$ ) are shown in Fig.41 proving the cancellation of the reactive power.

```

%First Method
% power factor
fi=atan(Id/Iq);
PF(i)=cos(fi);

% Active Power [kW]
Active_power1(i)=Ein*Iqff*cos(fi)/1000;

% Reactive Power
Reactive_power1(i)=Ein*Iqff*sin(fi)/1000;

% Second Method
Active_power2(i)=3*(Ed*Id+Eq*Iq)/2/1000;
Reactive_power2(i)=3*(Eq*Id-Ed*Iq)/2/1000;

% Third Method
Active_power3(i)=(Valfa*Ialfa+Vbeta*Ibeta)/1000;
Reactive_power3(i)=(Vbeta*Ialfa-Valfa*Ibeta)/1000;
    
```

The DC link voltage step response was obtained by using a DC link voltage test generator (Fig.42) under a load current variation between  $[0.65, 1.15] \times I_N$  (Fig.41),  $I_N$  being the rated value of the line current.

The performances of the active current inverter control are shown in Fig.41. The actual active current,  $I_q$ , accurately follows the reference  $I_{qref}$  (Fig.41). In Fig. 42 the performances of DC-link voltage controllers are shown. The trace of the A phase of the line current is in phase with A phase of the grid voltage, which clearly demonstrates the unity power factor

operation (Fig. 43). Comparative waveforms showing unity power factor operation during regeneration obtained from DC-AC power converter are shown in Fig. 43. For all three methods of active and reactive power deduction (Fig.44) the steady state values are the same, however the first method is more accurate in transient regime (Fig.44) (Gaiceanu, 2004b).

The 2nd degree DC link current estimator was implemented for a 37kVA power inverter. The dynamic performances of the DC load current estimator are presented (Gaiceanu, 2004a).

By an adequate choice of the estimator parameters an acceptable step response can be obtained (Fig.45).

Through simulation (Figs. 45-46) the real and the estimated DC link currents are obtained.

The power semiconductor active devices operate with a switching time  $T_s=125\mu s$ , and a  $2\mu s$  dead time. The converter specifications are given as follows: Supply voltage (line-to-line): 400V; Main frequency: 50Hz, Line current: 69A, Line inductance: 0.5 mH, DC bus capacitor: 1000  $\mu F$ , Ambient temperature 40°C,DC voltage reference: 690V.

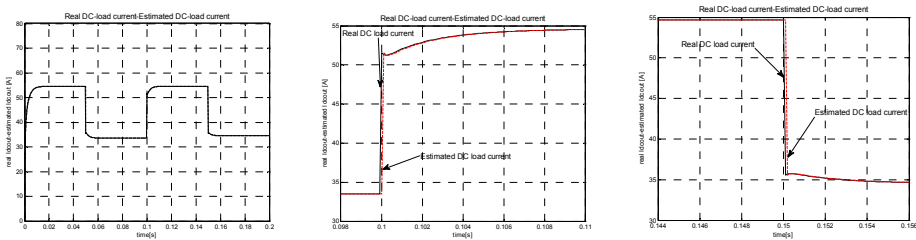


Figure 45. Simulation results. The real DC load current  $I_{dout}$ , the estimated DC link current  $\hat{I}_{dcout}$ .

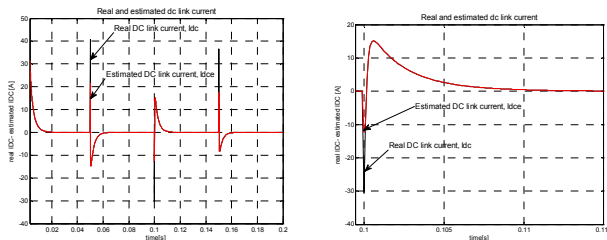


Figure 46. Simulation results. The real DC link current  $I_{dc}$ , the estimated DC link current  $\hat{I}_{dc}$ .

### 5. dSpace implementation

The PI Current Control in Synchronously Reference Frame is shown in Fig.47. The current regulators have two tasks: the error cancelling, and the modulation (the appropriate switching states are provided).

For an adequate tuning of the current regulators, the actual load current,  $i_A$ , accurately follows its reference  $i^*_A$  (Fig. 49), despite of an inappropriate tuning of the current controllers (Fig.48).

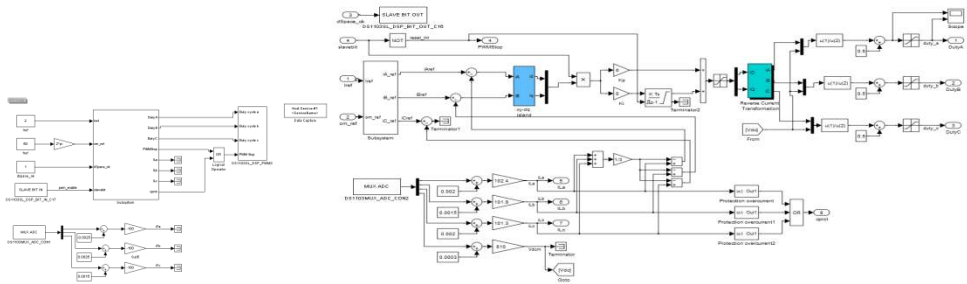


Figure 47. Real time implementation of the current control by using dSpace 1103 platform

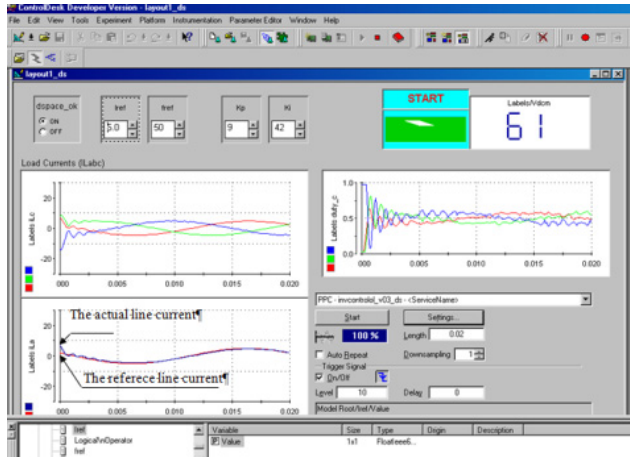


Figure 48. The three phase load currents, the corresponding duty cycles, the actual and the reference line currents for the inaccurate tuning of the current regulator parameters:  $K_p=9$ ,  $K_i=42$

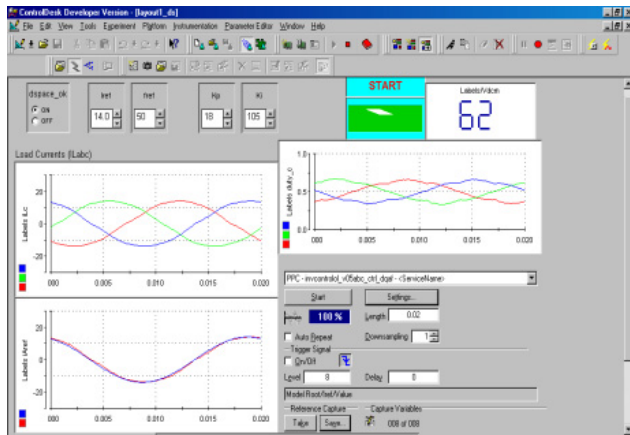


Figure 49. The three phase load currents, the corresponding duty cycles, the actual and the reference line currents for the accurate tuning of the current regulator parameters:  $K_p=18$ ,  $K_i=105$

## 6. Conclusions

The main outcomes of the chapter:

- The chapter pursues to increase the awareness of public regarding the renewable energy technologies through the open access, and to determine the researchers to implement renewable energy projects.
- The chapter will contribute the promotion of RES through the formation of experts so that these experts can later carry out RES projects with outstanding results.

The implicit longer term outcomes are related to:

1. Accurate models for fuel cells power systems.
2. New design of the adequate controllers for integrated systems, which will enable the efficient operation of such power inverters connected to the grid, with high stability in service and power quality.
3. The rapid prototyping through dSpace real time platform can prove very useful in medium and longer term for further modelling/investigation/development of similar systems.

The chapter will also bring contributions to the development of the theoretical knowledge if the following aspects are taken into account: the complexity of the issue, its interdisciplinary, the performance of an experimental model and the necessary theoretical knowledge of the interface solutions for the renewable system, in particular for fuel cells.

Through a proper control sinusoidal input current, a nearly unity power factor (0,998), bi-directional power flow, small (up to 5%) ripple in the DC-link voltage in any operated conditions, disturbance compensation capability, fast control response and high quality balanced three-phase output voltages were obtained. By using the load feed-forward component the input reference of the current is changed with load so that a better transient response is obtained. The proposed control was successfully implemented by the author on quasi direct AC-AC power converter (Gaiceanu M., 2004b) and based on the Matlab/Simulink software the simulation test has been performed for the modified topology of the grid power inverter. The experimental results (Figs. 48, 49) have been obtained by using dSpace platform (Fig.47). The second-degree DC load current estimator for DC-AC power converter system is developed in this chapter. Since the DC-AC power converter control by means of pulse-width modulation (PWM) is based on the power balance concept, its load power should be known. In order to overcome the measuring solution with well-known disadvantages, the load power can be estimated from the DC side by using the DC load current estimator. Thus, it is mandatory to have the information regarding the DC load current. The DC voltage regulation with good dynamic response is achieved even if DC capacitance is substantially reduced. This implies also the good accuracy of the DC link load current estimation.

### Author details

Marian Gaiceanu

*Dunarea de Jos University of Galati, Romania*

## 7. References

- Abou El-Maaty Metwally (2005). Modelling and Simulation of a Photovoltaic Fuel Cell Hybrid System) Kassel, Germany
- Candusso D. , Valero I.& Walter A. (2002). Modelling, control and simulation of a fuel cell based power supply system with energy management, IECON 2002 28<sup>th</sup> Annual Conference , pp.1294-1299
- COM(2006) Action Plan for Energy Efficiency: Realising the Potential, Available from [http://ec.europa.eu/energy/action\\_plan\\_energy\\_efficiency/doc/com\\_2006\\_0545\\_en.pdf](http://ec.europa.eu/energy/action_plan_energy_efficiency/doc/com_2006_0545_en.pdf)
- EREC, Renewable Energy Technology Roadmap (2008), Available from [http://www.erec.org/fileadmin/erec\\_docs/Documents/Publications/Renewable\\_Energy\\_Technology\\_Roadmap.pdf](http://www.erec.org/fileadmin/erec_docs/Documents/Publications/Renewable_Energy_Technology_Roadmap.pdf), pp2
- EREC, the European Renewable Energy Council (2011). Mapping Renewable Energy Pathways towards 2020, Available from [http://www.eufores.org/fileadmin/eufores/Projects/REPAP\\_2020/EREC-roadmap-V4.pdf](http://www.eufores.org/fileadmin/eufores/Projects/REPAP_2020/EREC-roadmap-V4.pdf)
- Gaiceanu M (2004b). AC-AC Converter System for AC Drives, *IEE Conference Publication Journal*, British Library, London, Publisher: Institution of Electrical Engineers, Vol. 2, no. 498, Printed in Great Britain by WRIGHTSONS, ISSN 0537-9989, pp 724-729
- Gaiceanu M. (2004a). A new load power estimator for quasi-sinusoidal ac-ac converter system," *Proceedings of the 9th International Conference on Optimization of Electrical and Electronic Equipments (OPTIM 2004)*, Vol. II: Power Electronics, Electrical Machines & Drives, ISBN 973-635-287-0, Brasov, May 20-21, pp.189-195, 2004
- Gaiceanu M. (2007a) Inverter Control for Three-Phase Grid Connected Fuel Cell Power System, *The 5th International IEEE Conference CPE 2007, Compatibility in Power Electronics Conference*, May 29- June 1, 2007, Gdansk, Poland, Power Electronics, 2007 Compatibility in, Conf Proceedings IEEE Product No.: EX1712, ISBN: 1-4244-1054-1
- Gaiceanu, M.& Fetecau G. (2007b). Grid connected Wind turbine-Fuel Cell Power System having Power Quality Issues, EPQU'07 Barcelona, pp.7-13, 2007. ISBN 978-84-690-9441-9
- Gulderin Hanifi (2005), Sliding Mode Control of DC-DC boost converter, *Journal of Applied Sciences* 5 (3): 588-592
- Ionescu Fl. et al (1997). *Electronica de putere. Modelare si simulare*, Editura Tehnica
- Padulles J., Ault G.W. & McDonald J.R. (2000). An integrated SOFC plant dynamic model for power systems simulation, *J. Power Sources* 86 495\_500
- Sul, S.K., & Lipo T.A. (1990). Design and performance of a high-frequency link induction motor drive operating at unity power factor," *IEEE Trans. Ind. Applicat.*, vol.26, no.3, pp. 434-440, May/June
- Uhrin, R.& Profumo F. (1994). Performance comparison of output power estimators used in AC/DC/AC converters, *Industrial Electronics, Control and Instrumentation*, IECON '94., 20th International Conference on, Volume 1, 5-9 Sept. 1994 Page(s):344 - 348 vol.1, 1994

Zhu Y. & Tomsovic K. (2002). Development of models for analyzing the load-following performance of microturbines and fuel cells, *Electric Power Systems Research* 62 (2002) 1\_11